Impact of symmetrized and Burt–Foreman Hamiltonians on spurious solutions and energy levels of InAs/GaAs quantum dots*

Gu Yong-Xian(谷永先), Yang Tao(杨 涛)†, Ji Hai-Ming(季海铭),
Xu Peng-Fei(徐鹏飞), and Wang Zhan-Guo(王占国)

Key Laboratory of Semiconductor Materials, Institute of Semiconductors, Chinese Academy of Sciences, P.O. Box 912, *Beijing* 100083, *China*

(Received 2 February 2010; revised manuscript received 1 March 2010)

We present a systematic investigation of calculating quantum dots (QDs) energy levels using the finite element method in the frame of the eight-band $\boldsymbol{k}\cdot\boldsymbol{p}$ method. Numerical results including piezoelectricity, electron and hole levels, as well as wave functions are achieved. In the calculation of energy levels, we do observe spurious solutions (SSs) no matter Burt–Foreman or symmetrized Hamiltonians are used. Different theories are used to analyse the SSs, we find that the ellipticity theory can give a better explanation for the origin of SSs and symmetrized Hamiltonian is easier to lead to SSs. The energy levels simulated with the two Hamiltonians are compared to each other after eliminating SSs, different Hamiltonians cause a larger difference on electron energy levels than that on hole energy levels and this difference decreases with the increase of QD size.

Keywords: quantum dot, symmetrized Hamiltonian, Burt–Foreman Hamiltonian, finite element method, spurious solutions

PACC: 8116D, 6322, 7125

1. Introduction

In recent years, semiconductor quantum dots (QDs) have attracted a lot of interest, not only because of their application in conventional optoelectronics,[1,2] but also their potential applications for quantum information processing.[3] Much work including growth, properties and applications has been done experimentally and theoretically. In particular, the development of single QD or QD molecule devices puts forward a demand for accurate calculation of electronic and optical properties of QDs.

The $\boldsymbol{k}\cdot\boldsymbol{p}$ theory was early proposed by Kane,[4] Luttinger and Kohn,[5] and developed to include stain interaction matrix by Bir and Pikus.[6] This model was originally applied to the description of electronic properties in bulk materials, then with some modifications it was applied to low dimensional heterostructures.[7−9] When the $\boldsymbol{k}\cdot\boldsymbol{p}$ theory is used to heterostructures, the k_i needs to be replaced by the operator $\hat{k} = -\mathrm{i}\partial/\partial x_i$, this procedure raises a problem[10,11] of the correct ordering of the operator with respect to the effective mass and strain parameters. Conventionally this problem is resolved by symmetrizing every matrix element of the Hamiltonian,[12,13] that is, making each matrix element a Hermitian operator. It was proved not to be necessary to make every matrix element Hermitian by Burt and Foreman,[10,11] although the Hamiltonian as a whole is always Hermitian.

In order to utilize the eight-band $\boldsymbol{k}\cdot\boldsymbol{p}$ method to calculate arbitrary practical QD shape, we must resort to a numerical method, such as the finite difference or finite element method. As we know, up to now most literature is related to the finite difference method while rarely using the finite element method which is thought to be more powerful for complex structures. No matter which numerical methods are used, the main difficulty in simulation with a numerical method is the spurious solutions (SSs) problem.[11,14−19] This issue is only widely studied in quantum well and quantum wire structures, and until now the comparison be-

*Project supported by the National High Technology Research and Development Program of China (Grant No. 2006AA03Z401), 'One-Hundred Talents Program' of the Chinese Academy of Sciences, and the National Natural Science Foundation of China (Grant No. 60876033).

†Corresponding author. E-mail: tyang@semi.ac.cn

© 2010 Chinese Physical Society and IOP Publishing Ltd

tween the symmetrized and Burt–Foreman Hamiltonians has only been carried out for quantum well, quantum wire and spherical dot.[20] In our simulation, we turn to the finite element method and analyse the phenomenon of SSs in QDs, and results calculated with symmetrized and Burt–Foreman Hamiltonian for QDs are compared to each other after eliminating SSs.

This paper is organized as follows: First, the numerical model is outlined in Subsection 2.1. Secondly, the strain and piezoelectricity including linear and quadratic parts are studied in Subsection 2.2, then thirdly the stain and total piezoelectricity are inserted into an eight-band $\boldsymbol{k}\cdot\boldsymbol{p}$ Hamiltonian to calculate the energy levels and wave functions in Subsection 2.3 in which the SSs problem is carefully investigated, such as the impact of different Hamiltonians on SSs. Fourthly, in Subsection 2.4 the results simulated with different Hamiltonians are compared to each other. At last this paper is concluded in Section 3.

2. Theory and calculations

2.1. Numerical method

In order to compare the results with other literatures calculated with the finite difference method,[7,21] the shape of QD is chosen to be a typical pyramid shape and it is easy to change to other shapes. The parameters of InAs and GaAs are taken from Refs. [7] and [21]. The InAs QD including 1.7-ML wetting layer, is embedded in GaAs material and the QD is grown on GaAs(001) surface. The extension of the simulation box is about two times larger than that of the QD in vertical and lateral directions. The effect of boundary conditions is thought to be small and the stain and wave functions are calculated with Dirichlet boundary conditions.

2.2. Stain and piezoelectricity

The stain plays an important role in the QD electrical and optical properties in two ways: First, it is directly added into the eight-band $\boldsymbol{k}\cdot\boldsymbol{p}$ Hamiltonian, which was systematically given by Bir and Pikus,[6] it will be discussed in Subsection 2.3. Secondly, stain can lead to piezoelectric effect which indirectly changes the energy levels and the wave functions of the electron and hole. With the consideration of piezoelectricity, the pyramid QD changes its symmetry from C_{4v} to C_{2v} so that the degeneracy of some states is lifted, such as the electron p-state splitting.

The stain distribution is calculated with the shrink fit procedure method,[22] which can be described as two steps: The initial state, the InAs pyramid is homogeneously strained with the lattice constant equal to that of substrate GaAs, while the substrate GaAs has no stain; After relaxation, the whole system reaches the equilibrium state, the elastic energy of the system achieves its minimum with the mesh points of finite element method getting proper displacement u_i, and the stain distribution is denoted as $\varepsilon_{ij}=\partial u_i/\partial x_j$.

When the stain is applied to a crystal lacking a centre of symmetry, such as InAs and GaAs, which have a zinc-blende structure, the crystal will result in electric polarization. This phenomenon is piezoelectricity.[13] The whole piezoelectricity can be divided into linear and quadratic parts.[21] The linear polarization is described by only one parameter e_{14},

$$\boldsymbol{P}_1 = 2e_{14}\begin{pmatrix}\varepsilon_{yz}\\ \varepsilon_{xz}\\ \varepsilon_{xy}\end{pmatrix}. \tag{1}$$

The quadratic part is related to three parameters B_{114}, B_{124} and B_{156},

$$\boldsymbol{P}_2 = 2B_{114}\begin{pmatrix}\varepsilon_{xx}\varepsilon_{yz}\\ \varepsilon_{yy}\varepsilon_{xz}\\ \varepsilon_{zz}\varepsilon_{xy}\end{pmatrix} + 2B_{124}\begin{pmatrix}\varepsilon_{yz}(\varepsilon_{yy}+\varepsilon_{zz})\\ \varepsilon_{xz}(\varepsilon_{xx}+\varepsilon_{zz})\\ \varepsilon_{xy}(\varepsilon_{xx}+\varepsilon_{yy})\end{pmatrix} + 4B_{156}\begin{pmatrix}\varepsilon_{xz}\varepsilon_{xy}\\ \varepsilon_{yz}\varepsilon_{xy}\\ \varepsilon_{yz}\varepsilon_{xz}\end{pmatrix}. \tag{2}$$

The piezoelectric charge density is obtained from the sum of $\boldsymbol{P}_1$ and $\boldsymbol{P}_2$,

$$\rho(\boldsymbol{r}) = -\boldsymbol{\nabla}\cdot(\boldsymbol{P}_1+\boldsymbol{P}_2). \tag{3}$$

The piezoelectric potential $V_{\rm p}(\boldsymbol{r})$ arises from solving Possion equation,

$$\rho(\boldsymbol{r}) = \varepsilon_0\boldsymbol{\nabla}\cdot[\varepsilon_{\rm s}(\boldsymbol{r})\nabla V_{\rm p}(\boldsymbol{r})], \tag{4}$$

where ε_0 is vacuum permittivity and $\varepsilon_{\rm s}(\boldsymbol{r})$ is static dielectric constant. In this paper, $\varepsilon_{\rm s}(\boldsymbol{r})$ is a step function with regard to GaAs and InAs.

The piezoelectric potential of pyramid QD with base length 13.6 nm including linear, quadratic and total polarization is given in Fig. 1, black (gray) surface stands for isosurface of 30 mV (−30 mV). The results are consistant with those presented by Schliwa.[21] The linear and quadratic part have opposite contribution to the total piezoelectricity and the former is more widespread. The anisotropy between [110] and [1–10] directions lowers the the symmetry of the system from C_{4v} to C_{2v} and leads to the redistribution of wave functions of electron and hole.

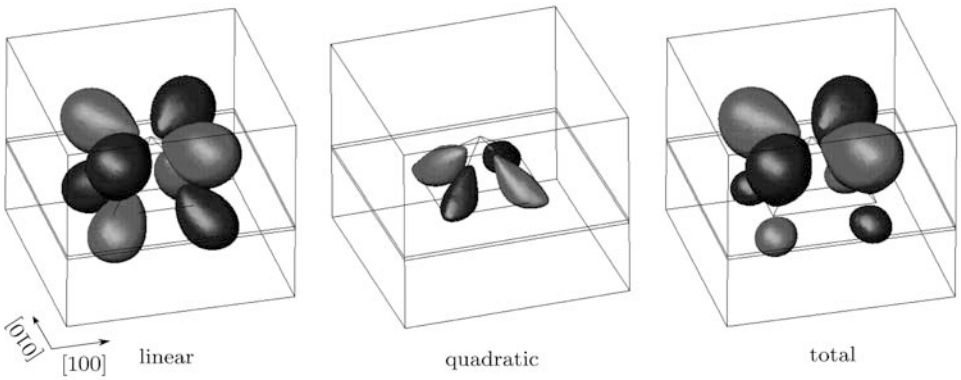


Fig. 1. Piezoelectric potential of pyramid QD with base length 13.6 nm, black (gray) area stands for isosurface of 30 mV (–30 mV).

2.3. Eight-band $k \cdot p$ theory

2.3.1. Symmetrized and Burt–Foreman Hamiltonian

When the Hamiltonian in Eq. (A2) in Appendix A is applied to heterostructure, in most papers incorrect symmetrized Hamiltonian is adopted. The symmetrized procedure can be described as:[12]

$$\begin{aligned} &Qk_i \to (Q\hat{k}_i + \hat{k}_i Q)/2, \\ &Qk_ik_j \to (\hat{k}_i Q\hat{k}_j + \hat{k}_j Q\hat{k}_i)/2, \\ &i, j = x, y, z, \end{aligned}$$

where Q stands for a Kane parameter or a stain component which is a function of spatial location. According to the theory of Burt and Foreman,[10,11] an unsymmetrized exact Hamiltonian is obtained by a more sophisticated replacement. In Eq. (A3), the diagonal terms are still to be treated according to the symmetrized procedure

$$Qk_i^2 = \hat{k}_i Q\hat{k}_i,$$

the upper triangular matrix element

$$N'k_ik_j \to \hat{k}_i N_+ \hat{k}_j + \hat{k}_j N_- \hat{k}_i,$$

where $N_- = M - \hbar^2/2m_0$ and $N_+ = N' - N_-$, the lower triangular matrix element

$$N'k_ik_j \to \hat{k}_j N_+ \hat{k}_i + \hat{k}_i N_- \hat{k}_j.$$

In Eq. (A4), the upper triangular matrix element

$$\mathrm{i}\,Pk_i - \mathrm{i}\,P\varepsilon_{ij}k_j \to \mathrm{i}\,P\hat{k}_i - \mathrm{i}\,P\varepsilon_{ij}\hat{k}_j,$$

the lower triangular matrix element

$$-\mathrm{i}\,Pk_i + \mathrm{i}\,P\varepsilon_{ij}k_j \to -\mathrm{i}\,\hat{k}_i P + \mathrm{i}\,\hat{k}_j P\varepsilon_{ij}.$$

2.3.2. Spurious solutions

The appearance of SSs is a long standing problem. In our simulation with the finite element method, we do observe SSs using all parameters from Ref. [21]

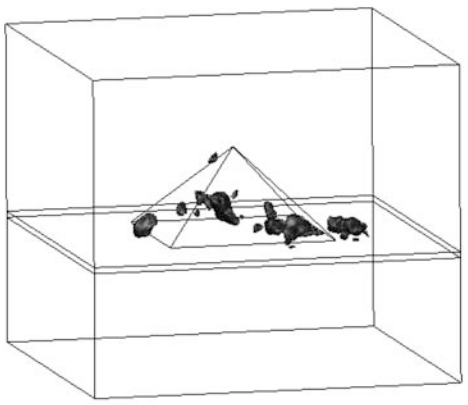


Fig. 2. Wave function of SSs. The wave functions are very irregular and appear at the interface between InAs and GaAs.

the no matter symmetrized or unsymmetrized (Burt–Foreman) Hamiltonian is used. The wave functions are very irregular and appear at the interface between InAs and GaAs as illustrated in Fig. 2. In order to overcome this difficulty, many studies have been done.[11,14−19] There are several viewpoints about origin and elimination of SSs. As we know, there is no detailed analysis about this phenomenon of SSs in QD, most papers concentrated on the SSs in calculation of quantum well or superlattice structures.

In Refs. [16] and [19], SSs were considered to be due to the energy band in bulk material calculated with eight-band $\boldsymbol{k}\cdot\boldsymbol{p}$ method unphysically bending toward the energy gap. Based on this theory, the wave vector cutoff method[16,19] is adopted when the plane-wave expansion method is used, that is to restrict the plane-wave expansion set containing first Brillouin-zone components only. Figure 3 depicts the diagram of the band structure of GaAs (a) and InAs (b) using the eight-band $\boldsymbol{k}\cdot\boldsymbol{p}$ method, the conduction band (valence band) of GaAs (InAs) bends toward the energy gap at large wave vector k when the original $E_{\rm p}$ (28 meV for GaAs, 22.204 meV for InAs) from Ref. [21] is used.

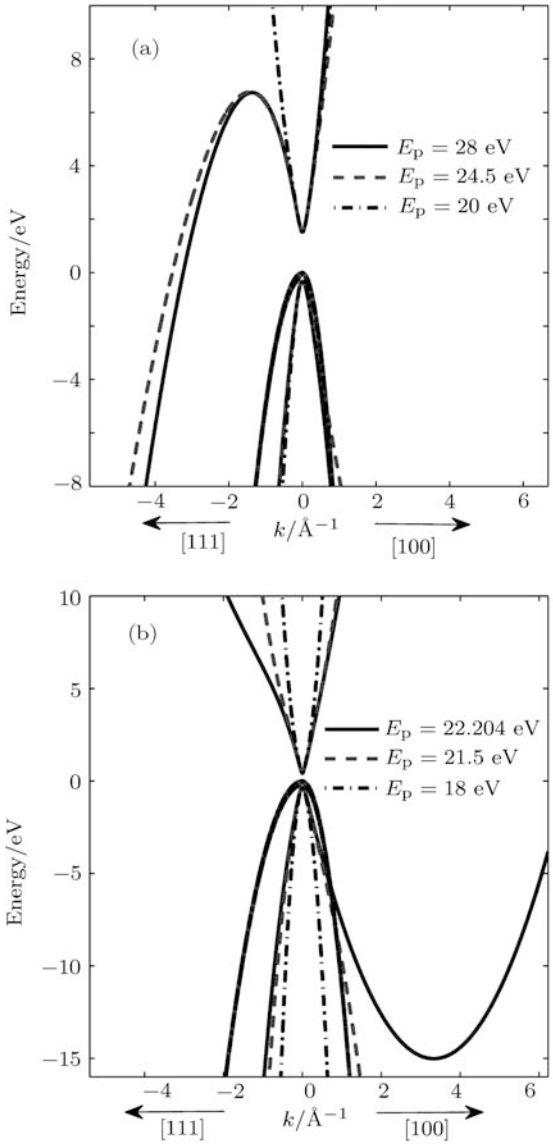


Fig. 3. Diagram of the band structure of GaAs (a) and InAs (b) using the eight-band $\boldsymbol{k}\cdot\boldsymbol{p}$ method with different $E_{\rm p}$ values. The band structure with original $E_{\rm p}$ from Ref. [21] is plotted with solid line. The k range is five times larger than the first Brillouin zone.

From the mathematical viewpoint, Veprek[18] pointed out that SSs were due to the lack of ellipticity of the Hamiltonian and proposed a criteria to judge the ellipticity of Hamiltonian.

$$\begin{aligned} &A' > 0, \quad M - N_- < 0, \quad M + N_- < 0, \\ &L' - N_+ < 0, \quad L' + 2N_+ < 0. \end{aligned} \tag{5}$$

The Hamiltonian is elliptic if this criterion is met. In fact this criterion generally cannot be met and in practical applications it is too strict, so the degree of closeness to the ellipticity can be estimated by the ratio

$$\rho = \left| \frac{\sum\limits_{i,\lambda_i>0} \lambda_i}{\sum\limits_{j,\lambda_j<0} \lambda_j} \right|, \tag{6}$$

where λ_i is the value of

$$\begin{aligned} &-A'(3\times), \quad M - N_-(3\times), \quad M + N_-(3\times), \\ &L' - N_+(2\times), \quad L' + 2N_+(1\times). \end{aligned} \tag{7}$$

Compared to Ref. [18], we add $-A'(3\times)$ into Eq. (6) to describe the ellipticity. If equation (5) is met, the ρ in Eq. (6) will be zero. From Fig. 4, it is found that the ρ decreases with the decrease of $E_{\rm p}$, so SSs can be eliminated by reducing $E_{\rm p}$. This method is considered to have little effect on actual results, because A', L', M, N', N_+, N_-, and P all change with $E_{\rm p}$ such that the new set of parameters can still well fit the energy band structure of bulk materials near the Γ point. It can be seen from Fig. 3 that the energy bands calculated with different $E_{\rm p}$ coincide well near the Γ point. In addition, the ellipticity is not affected by piezoelectricity because the ellipticity is determined by the parameters of quadratic part of k_i.

In our simulation, we use reduced $E_{\rm p}$ in GaAs and InAs to eliminate SSs, because the wave vector cutoff method is only suitable for simple structures, such as quantum well, superlattice and cylindrical quantum dot calculated using plane-wave expansion method. In

Ref. [11], in order to eliminate SSs, A' is set to be zero, and

$$E_{\rm p} = \frac{3m_0/m_{\rm e}^*}{2/E_{\rm g} + 1/(E_{\rm g} + \Delta)}. \quad (8)$$

In fact, this method is equivalent to reduce the $E_{\rm p}$ value and can be regarded as a special case of the ellipticity theory. Using Eq. (8), the $E_{\rm p}$ for GaAs and InAs are 24.24 meV and 22.04 meV respectively, but still can cause SSs. According to the analysis below, the $E_{\rm p}$ for InAs still need to be reduced. By trying different $E_{\rm p}$ for GaAs and InAs, we find that there are no SSs with $E_{\rm p}$ being 24.5 meV for GaAs and 21.5 meV for InAs, the corresponding wave functions are given in Figs. 5 and 6 and energy levels are given in Fig. 7 which will be discussed in detail in Subsection 2.4. In order to investigate the origin of SSs, we take a fixed $E_{\rm p}$ value for one material, then reduce the $E_{\rm p}$ of the other material by 0.1 meV for each calculation from the original value to zero. The fixed $E_{\rm p}$ values for GaAs and InAs are respectively 24.5 meV and 21.5 meV. The whole $E_{\rm p}$ range is divided into regions containing and not containing SSs as displayed in Table 1. The SSs disappear when the $E_{\rm p}$ of GaAs is less than 24.6 meV for both symmetrized and Burt–Foreman Hamiltonians. When the $E_{\rm p}$ of InAs is less than 21.6 meV, the SSs can be eliminated for Burt–Foreman Hamiltonian, but for symmetrized Hamiltonian the SSs arise again when $E_{\rm p}$ is less than 18.6 meV. This can be explained by the increase of ρ of InAs with the decrease of $E_{\rm p}$ when the $E_{\rm p}$ is less than 20.6 meV, and this phenomenon cannot be explained by the energy band bending toward the band gap in bulk material, because when the $E_{\rm p}$ is less than a certain value there is no bending toward the band gap as illustrated in Fig. 4.

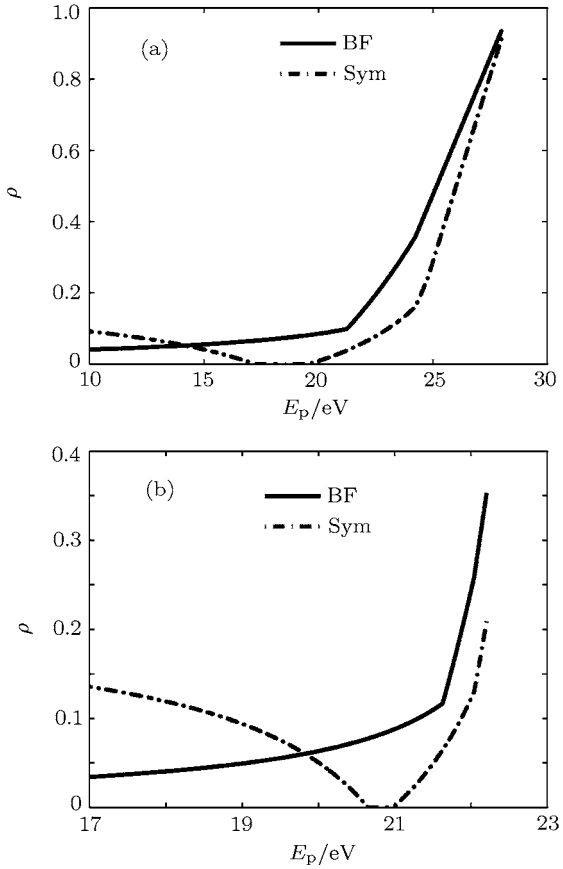


Fig. 4. Ellipticity of the Hamiltonian for GaAs (a) and InAs (b) as a function of the $E_{\rm p}$ value. All parameters are taken from Ref. [21].

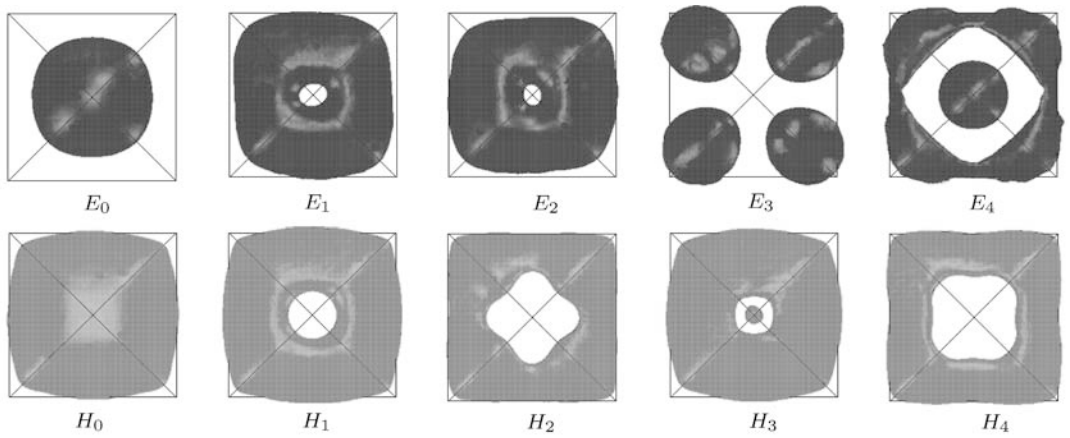


Fig. 5. Probability density isosurfaces (25% of the peak value) of electron and hole using Burt–Foreman Hamiltonian without piezoelectricity, pyramid base length 13.6 nm.

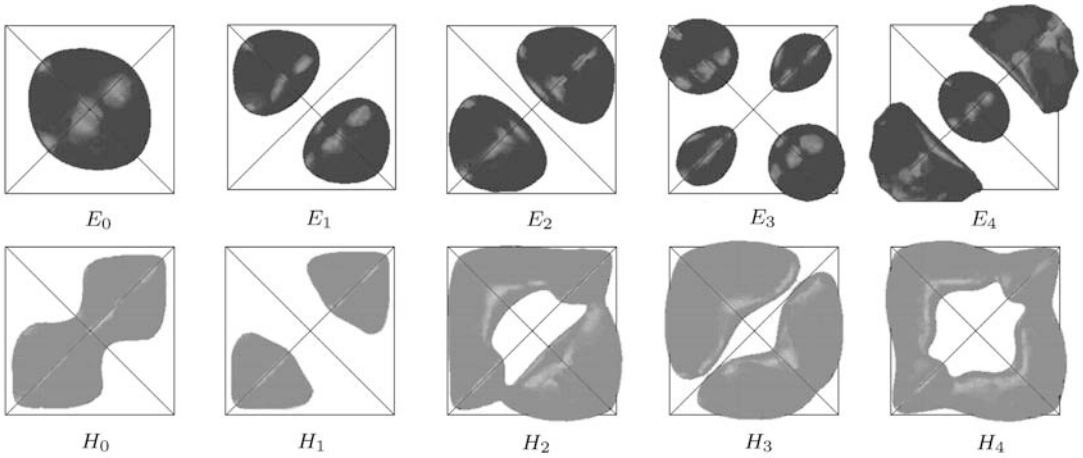


Fig. 6. Probability density isosurfaces (25% of the peak value) of electron and hole using Burt–Foreman Hamiltonian with piezoelectricity, pyramid base length 13.6 nm.

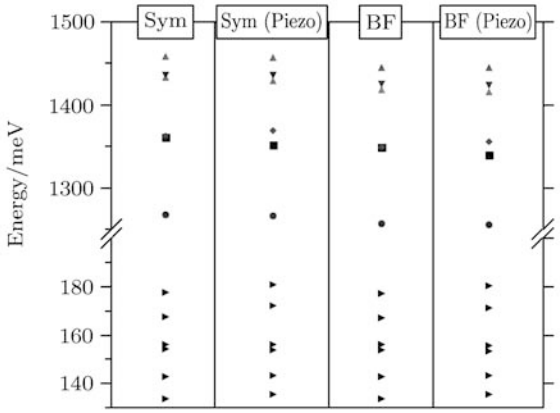


Fig. 7. Single-particle energy levels with symmetric Hamiltonian or Burt–Foreman Hamiltonian, with or without piezoelectricity. The $E_{\rm p}$ of GaAs and InAs are 24.5 meV and 21.5 meV respectively, pyramid base length 13.6 nm.

It is noteworthy that the conversion from containing SSs to not containing SSs is not a sudden change. Take InAs calculated with symmetrized Hamiltonian as an example, when $E_{\rm p}$ is a little larger than 21.5 meV, the SSs only appear in high energy levels in conduction band. The SSs arise again in high energy levels in valence band when the $E_{\rm p}$ is a little less than 18.5 meV. The more $E_{\rm p}$ deviated from the stable region without SSs, the more severe the SSs problem. In addition, we find that the ρ of GaAs in the case of symmetrized Hamiltonian increases as the $E_{\rm p}$ decreases when the $E_{\rm p}$ is less than 17.22 meV, but the SSs do not appear, this is due to the fact that the increase extent of ρ is small.

The ellipticity theory can explain the origin of SSs, but it cannot explain why SSs disappear at the same $E_{\rm p}$ (24.5 meV for GaAs and 21.5 meV for InAs) corresponding to which the ρ values are not equal for different Hamiltonians. This may be due to two reasons: Firstly, equation (6) is only an estimation of ellipticity. Secondly, the SSs are also affected by other factors, such as energy bands bending toward energy gap in bulk material mentioned above and finite element mesh division which is observed in some cases in our calculation. So in practice we still need to tentatively choose a proper $E_{\rm p}$.

Table 1. Analysis of SSs, the whole $E_{\rm p}$ range is divided into regions containing and not containing SSs.

material	Hamiltonian	$E_{\rm p}$ (meV) with SSs	$E_{\rm p}$ (meV) without SSs
GaAs	Sym	28–24.6	24.5–0
GaAs	BF	28–24.6	24.5–0
InAs	Sym	22.204–21.6, 18.5–0	21.5–18.6
InAs	BF	22.204–21.6	21.5–0

2.4. Results and comparison

In Fig. 5, wave functions of electron and hole calculated using Burt–Foreman Hamiltonian without piezoelectricity are given. The base length of QD is 13.6 nm. The surfaces stand for isosurfaces of 25% of the peak value of probability density. In Fig. 6, piezoelectricity is included. When considering the piezoelectricity, electron tends to stay in [1–10] direction, while hole tends to stay in [110] direction. Every energy level is twofold degenerate because of spin up and spin down. The energies of E_1 and E_2 are almost identical without piezoelectricity, while they have a splitting (p-state splitting) about 16 meV when considering the piezoelectricity as displayed in Fig. 7. Additionally, with piezoelectricity, H_0 and H_1 wave functions significantly change their shapes, which will evidently affect the luminescence properties of QD, such as optical anisotropy in [110] and [1–10] directions. By comparison, the wave functions of hole are more sensitive to piezoelectricity than that of electron, this is mainly because hole has a more heavy effective mass than electron and tends to change its wave function to adapt to piezoelectric potential distribution.

The energy levels calculated with symmetrized or Burt–Foreman Hamiltonian, with or without piezoelectricity for base length 13.6 nm are presented in Fig. 7. The corresponding wave functions simulated with Burt–Foreman Hamiltonian are given in Figs. 5 and 6. The $E_{\rm p}$ of GaAs and InAs are 24.5 meV and 21.5 meV respectively. All results are calculated with the same meshes distribution of the finite element method. When piezoelectricity is considered, the energy of electron ground state E_0 decreases by 1.3 meV and the energy of hole ground state H_0 increases by 3.3 meV, so the transition energy between E_0 and H_0 decreases by about 4.6 meV. The change of energy levels are determined by two factors: Because of piezoelectricity, electron (hole) tends to stay in [1–10] ([110]) direction, the quantum confinement effect is enhanced, but simultaneously there is negative piezoelectric potential in the [1–10] ([110]) direction. We find that the effect of negative piezoelectric potential is slightly larger than the enhanced quantum confinement, so both electron and hole levels change tending to decrease transition energy. The energy level E_0 simulated with Burt–Foreman Hamiltonian decreases by about 9.8 meV comparing to that with symmetrized Hamiltonian, and hole energies decrease by about 0.6 meV, the transition energy between E_0 and H_0 decrease by about 9.2 meV, so different Hamiltonians mainly affect the energy levels of electron. Table 2 denotes the energy difference of E_0 and H_0 between two Hamiltonians for different base lengths, compared to the hole different Hamiltonians leads to a larger difference on energy levels of electron and this difference decreases with the increase of QD size. This is in agreement with the results in Ref. [20], as the size is decreased the wave functions will feel the interface more and more.

Table 2. The energy difference of E_0 and H_0 between two Hamiltonians for different base lengths.

base length/nm	E_0 (Sym)–E_0(BF)/meV	H_0 (Sym)–H_0(BF)/meV
10.2	13.14	0.66
13.6	9.85	0.62
17.0	7.03	0.61
20.4	5.20	0.59

Electron and hole energy levels of different base lengths calculated with Burt–Foreman Hamiltonian are given in Fig. 8. The p-state splitting (energy splitting between E_1 and E_2) increases with the increase of base length. Table 3 gives the detailed values of some typical sizes. By comparing the results with Fig. 7 in Ref. [13] which is simulated with symmetrized Hamiltonian using finite difference method, the energy difference of the electron is larger than that of the hole which is consistent with our previous analysis. On the whole, the two results coincide very well. It is difficult to analyse in detail because the comparison here is more complicated caused by three factors: One is the different numerical methods and different mesh divisions, the second is different Hamiltonians and the third is different $E_{\rm p}$ values for GaAs and InAs.

Table 3. The p-state splitting as a function of base length of pyramid QD, it increases with the increase of base length.

base length/nm	10.2	13.6	17	20.4
p-state splitting/meV	8.8	16.2	24.7	29.5

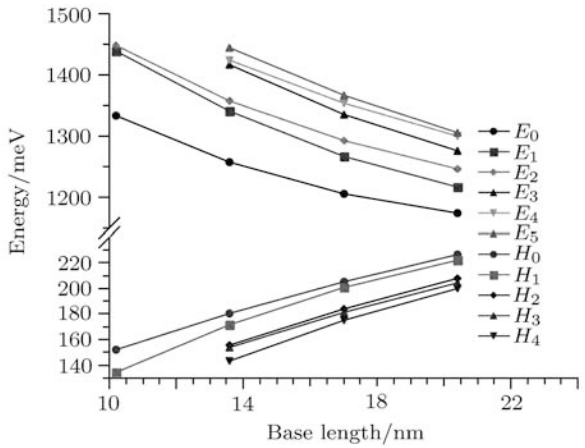


Fig. 8. Electron and hole energy levels of different base length pyramid QD, calculated with Burt–Foreman Hamiltonian.

3. Conclusion

We systematically calculated the stain, piezoelectricity and the single-particle energy levels and wave functions of electron and hole in InAs/GaAs QD with the finite element method. The appearance of SSs are carefully studied by reducing $E_{\rm p}$ in GaAs and InAs. We concluded that the SSs are mainly due to the lack of ellipticity of the Hamiltonian and symmetrized Hamiltonian is easier to lead to SSs. But in practice we still need to tentatively choose a proper reduced $E_{\rm p}$. We compared the results calculated with different Hamiltonians, compared to the hole, different Hamiltonians have a larger impact on energy levels of electron and this impact decreases with increase of QD base length.

Appendix: Eight-band $k \cdot p$ Hamiltonian

In this paper, we follow Kane's basis of atomic like states:

$$(|s\uparrow\rangle, |x\uparrow\rangle, |y\uparrow\rangle, |z\uparrow\rangle, |s\downarrow\rangle, |x\downarrow\rangle, |y\downarrow\rangle, |z\downarrow\rangle)^{\rm T}. \tag{A1}$$

In the basis, the Hamiltonian[12,13] can be described by three parts with respect to the order of k_i:

$$H = \begin{bmatrix} H_2 & \\ & H_2 \end{bmatrix} + \begin{bmatrix} H_1 & \\ & H_1 \end{bmatrix} + H_0, \tag{A2}$$

where H_2 and H_1 read as

$$H_2 = \begin{bmatrix} A'k^2 & 0 & 0 & 0 \\ 0 & L'k_x^2 + M(k_y^2 + k_z^2) & N'k_xk_y & N'k_xk_z \\ 0 & N'k_xk_y & L'k_y^2 + M(k_x^2 + k_z^2) & N'k_yk_z \\ 0 & N'k_xk_z & N'k_yk_z & L'k_z^2 + M(k_x^2 + k_y^2) \end{bmatrix}, \tag{A3}$$

$$H_1 = \begin{bmatrix} 0 & {\rm i}Pk_x - {\rm i}P\varepsilon_{xj}k_j & {\rm i}Pk_y - {\rm i}P\varepsilon_{yj}k_j & {\rm i}Pk_z - {\rm i}P\varepsilon_{zj}k_j \\ -{\rm i}Pk_x + {\rm i}P\varepsilon_{xj}k_j & 0 & 0 & 0 \\ -{\rm i}Pk_y + {\rm i}P\varepsilon_{yj}k_j & 0 & 0 & 0 \\ -{\rm i}Pk_z + {\rm i}P\varepsilon_{zj}k_j & 0 & 0 & 0 \end{bmatrix}. \tag{A4}$$

The constant matrix H_0 reads as

$$H_0 = \begin{bmatrix} G & \Gamma \\ -\Gamma^* & G^* \end{bmatrix}, \tag{A5}$$

the asterisk denotes the complex conjugation. Where

$$G = \begin{bmatrix} E_c + a_c(\varepsilon_{xx} + \varepsilon_{yy} + \varepsilon_{zz}) & 0 & 0 & 0 \\ 0 & E'_{\rm v} + l\varepsilon_{xx} + m(\varepsilon_{yy} + \varepsilon_{zz}) & n\varepsilon_{xy} - {\rm i}\Delta/3 & n\varepsilon_{xz} \\ 0 & n\varepsilon_{xy} + {\rm i}\Delta/3 & E'_{\rm v} + l\varepsilon_{yy} + m(\varepsilon_{xx} + \varepsilon_{zz}) & n\varepsilon_{yz} \\ 0 & n\varepsilon_{xz} & n\varepsilon_{yz} & E'_{\rm v} + l\varepsilon_{zz} + m(\varepsilon_{xx} + \varepsilon_{yy}) \end{bmatrix}, \tag{A6}$$

$$\Gamma = \begin{bmatrix} 0 & 0 & 0 & 0 \\ 0 & 0 & 0 & \Delta/3 \\ 0 & 0 & 0 & -\mathrm{i}\,\Delta/3 \\ 0 & -\Delta/3 & \mathrm{i}\,\Delta/3 & 0 \end{bmatrix}. \quad \text{(A7)}$$

The parameters that enter into Eq. (A2) are calculated as follows:

$$\begin{aligned} E_{\mathrm{c}} &= E_{\mathrm{v}} + E_{\mathrm{g}} - eV_{\mathrm{p}}, \\ E'_{\mathrm{v}} &= E_{\mathrm{v}} - \Delta/3 - eV_{\mathrm{p}}, \\ A' &= \frac{\hbar^2}{2m_0}\left(\frac{m_0}{m_{\mathrm{e}}^*} - \frac{E_{\mathrm{p}}}{E_{\mathrm{g}}}\frac{E_{\mathrm{g}} + 2\Delta/3}{E_{\mathrm{g}} + \Delta}\right), \\ P &= \sqrt{\frac{\hbar^2}{2m_0}E_{\mathrm{p}}}, \\ L' &= \frac{P^2}{E_{\mathrm{g}}} - \frac{\hbar^2}{2m_0}(\gamma_1 + 4\gamma_2), \\ M &= -\frac{\hbar^2}{2m_0}(\gamma_1 - 2\gamma_2), \\ N' &= \frac{P^2}{E_{\mathrm{g}}} - \frac{3\hbar^2}{m_0}\gamma_3, \\ l &= a_{\mathrm{c}} + 2b_{\mathrm{v}}, \\ m &= a_{\mathrm{c}} - b_{\mathrm{v}}, \\ n &= \sqrt{3}d_{\mathrm{v}}. \end{aligned}$$

The parameters appear on the right-hand side of the above equations are depicted in Table 4.

Table 4. Definition of parameters.

V_{p}	piezoelectric potential
E_{v}	valence band edge
E_{g}	fundamental band gap
Δ	spin–orbit splitting energy
m_0	free electron mass
m_{e}^*	electron effective mass in bulk material
E_{p}	optical matrix or band mixing parameter
$\gamma_1, \gamma_2, \gamma_3$	Luttinger parameters for six-band $\boldsymbol{k}\cdot\boldsymbol{p}$ method
a_{c}	hydrostatic conduction band deformation potential
b_{v}	hydrostatic valence band deformation potential
d_{v}	shear deformation potential

There are two main differences about the denotation of L', M, N' in different literatures. The first has to do with the extra factor of 1 in L', M in Ref. [12]. Because the Hamiltonian in Refs. [12] and [13] has included the contribution from the free-electron mass, so the extra factor of 1 in Ref. [12] should be omitted. The second difference has to do with the extra factors of Δ in the denominators of Bahder's[23] formulas. This is essentially due to an incorrect application of perturbation theory. The error was studied in some detail by Boujdaria[24] who demonstrated numerically that Bahder's approach leads to significant error.

References

[1] Bimberg D, Kirstaedter N, Ledentsov N, Alferov Z, Kop'ev P and Ustinov V 1997 *IEEE J. Select. Topics Quantum Electron.* **3** 196

[2] Lü X Q, Jin P and Wang Z G 2010 *Chin. Phys.* B **19** 018104

[3] Li H J, Sun J K and Xiao J L 2010 *Chin. Phys.* B **19** 010314

[4] Kane E O *Handbook on Semiconductors* Vol. I ed. Paul W 1982 (Amsterdam: North Holland)

[5] Luttinger J M and Kohn W 1955 *Phys. Rev.* **97** 869

[6] Bir G L and Pikus G E 1974 *Symmetry and Strain-induced Effects in Semiconductors* (New York: Wiley)

[7] Stier O, Grundmann M and Bimberg D 1999 *Phys. Rev.* B **59** 5688

[8] Chuang S L 1991 *Phys. Rev.* B **43** 9649

[9] Baraff G A and Gershoni D 1991 *Phys. Rev.* B **43** 4011

[10] Burt M G 1992 *J. Phys.: Condens. Matter* **4** 6651

[11] Foreman B A 1997 *Phys. Rev.* B **56** R12748

[12] Stier O 2000 *Electronic and Optical Properties of Quantum Dots and Wires* (Berlin: Wissenschaft and Technik Verlag)

[13] Schliwa A 2007 *Electronic Properties of Self-organized Quantum Dots* Ph.D. Thesis (Berlin: The Technical University of Berlin)

[14] White S R and Sham L J 1981 *Phys. Rev. Lett.* **47** 879

[15] Cartoixa X, Ting D Z Y and McGill T C 2003 *J. Appl. Phys.* **93** 3974

[16] Yang W and Chang K 2005 *Phys. Rev.* B **72** 233309

[17] Foreman B A 2007 *Phys. Rev.* B **75** 235331

[18] Veprek R G, Steiger S and Witzigmann B 2007 *Phys. Rev.* B **76** 165320

[19] Lassen B, Melnik R V N and Willatzen M 2009 *Commun. Comput. Phys.* **6** 699

[20] Lassen B, Voon L C L Y, Willatzen M and Melnik R 2004 *Solid State Commun.* **132** 141

[21] Schliwa A, Winkelnkemper M and Bimberg D 2007 *Phys. Rev.* B **76** 205324

[22] Lassen B, Willatzen M, Barettin D, Melnik R V N and Voon L C L Y 2008 *J. Phys.: Conference Series* **107** 012008

[23] Bahder T B 1990 *Phys. Rev.* B **41** 11992

[24] Boujdaria K, Ridene S and Fishman G 2001 *Phys. Rev.* B **63** 235302